^{57}Fe Mössbauer spectroscopy study of cycloidal spin arrangements and magnetic transitions in $BiFe_{1-x}Co_xO_3$

A. V. Sobolev,[1] V. S. Rusakov,[1] A. M. Gapochka,[1] I. S. Glazkova,[1] T. V. Gubaidulina,[1] M. E. Matsnev,[1] A. A. Belik,[2] and I. A. Presniakov[1]

[1]*M.V. Lomonosov Moscow State University, Moscow 119991, Russia*

[2]*International Center for Materials Nanoarchitectonics (WPI-MANA), National Institute for Materials Science (NIMS), Namiki 1-1, Tsukuba, Ibaraki 305-0044, Japan*

(Received 28 March 2020; revised manuscript received 23 April 2020; accepted 20 May 2020; published 5 June 2020)

We report results of a ^{57}Fe Mössbauer study focused on Co-substituted $BiFe_{1-x}Co_xO_3$ ($x = 0.05$). The experimental spectra were analyzed assuming the space-modulated cycloidal magnetic structure with high values of the anharmonicity parameter $m = 0.47-0.92$ (at 4.7 K). The m parameter increases with increasing temperature to reach its maximum value ($m \approx 1$) for $x = 0.10, 0.15$ corresponding to the transition to a collinear antiferromagnetic structure of easy-plane type ($\mu_{Fe} \perp c_h$). Such an unusual trend of the anharmonicity parameter $m(T)$ increasing with temperature was well reproduced by the molecular field model in which the low-spin to intermediate-spin transition of Co^{3+} is assumed. At low cobalt content, $BiFe_{0.95}Co_{0.05}O_3$, the cycloidal structure is retained but with a very high degree of anharmonicity, corresponding to the nearly collinear spin order.

DOI: 10.1103/PhysRevB.101.224409

I. INTRODUCTION

Among many magnetoelectric multiferroics, the perovskitelike bismuth ferrite $BiFeO_3$ is an extensively studied material, which exhibits antiferromagnetic ordering ($T_N \approx 650$ K) and ferroelectric transition ($T_C \approx 1100$ K) well above room temperature [1]. However, while $BiFeO_3$ is ferroelectric and is characterized by very high spontaneous polarization, its magnetization and magnetoelectric coupling are disappointingly smaller than the values that would be useful for application. This is because the cycloidal spin structure is superimposed on the antiferromagnetic order in iron sublattices [1,2]. The average magnetization is then equal to zero, which makes it impossible to efficiently control the electric properties via magnetic action and vice versa. In order to enhance some weak characteristics that are insufficient for practical application, it is possible to use partial replacement of Fe^{3+} in $BiFe_{1-x}M_xO_3$ with iso- or heterovalent M^{m+} ions, which can suppress the cycloidal spin structure [3,4]. For example, suppression of the cycloidal structure was observed when iron was partially substituted for isovalent ions $M^{3+} = Cr^{3+}$, Mn^{3+}, and Sc^{3+} [5,6]. The same behavior was observed in powder Co-substituted $BiFe_{1-x}Co_xO_3$ ($0.02 \leqslant x \leqslant 0.2$) [7–10] and epitaxial thin films [11–14], which manifest a magnetic phase transition from a low-temperature cycloidal modulation to an antiferromagnetic (AFM) G-type structure with canted ferromagnetism [12]. Obviously, this transition is the result of a delicate compromise between the magnetocrystalline anisotropy, competing isotropic and anisotropic exchanges, and magnetoelectric interactions. Although there are many reports [13,14] concerning the magnetism in Co-substituted $BiFeO_3$, the origin of the cycloidal modulation and its temperature-dependent evolution to a collinear high-temperature G-type phase is an important subject with several currently unresolved issues. Moreover, Co^{3+} ions can undergo the thermally induced spin transitions from the low-spin (LS) to high-spin (HS) state via the intermediate-spin (IS) state in perovskites [15]. The Co^{3+} spin states arise from the competition between crystal-field effects and Hund's exchange interactions, so a variety of interesting physics may be witnessed for partial substitution of Fe^{3+} with Co^{3+} in the noncollinear magnetic order.

^{57}Fe Mössbauer spectroscopy is a powerful local method for studying the electronic state, crystalline environment, and magnetic interactions of iron in solids. This method was used for studying the Co-substituted ferrites $BiFe_{1-x}Co_xO_3$ [8,11,16]. Nevertheless, in the cited Mössbauer studies [8,11], the complex magnetic hyperfine structure of ^{57}Fe spectra measured at $T < T_N$ was described as a superposition of two Zeeman partial components, which could be associated with the formation of two nonequivalent magnetic iron sites. Based on this "discrete" two-component model, it was assumed [11] that the collinear and cycloidal phases coexist. The anharmonicity in cycloidal modulation was not considered in these studies. This model has essential disadvantages although a good fit of the experimental Mössbauer spectra. The most important point is the lack of experimental data that prove the formation of two magnetic iron sites at low temperatures. The inhomogeneous environment of iron associated with various local configurations $\{(6-n)Fe^{3+}, nCo^{3+}\}$ was not taken into account. In addition, this approach does not take into account the cycloidal ordering of iron: Therefore, it can only qualitatively describe the profile of the experimental spectra but is not able to accurately reproduce all of their features.

In the present work, we propose an approach to the description of the ^{57}Fe Mössbauer spectra of $BiFe_{1-x}Co_xO_3$ ($0 < x \leqslant 0.15$) taking into account the spatially modulated spin

 ©2020 American Physical Society

ordering at $T \leqslant T_N$. We have shown that it is impossible to fit the spectra at $T \ll T_N$ using the simple spiral model. Instead, the bunched spiral model has provided very good fits. Earlier, this approach was successfully used to analyze the ^{57}Fe Mössbauer spectra of $BiFeO_3$ [17–22], $BiFe_{1-x}M_xO_3$ (M = Sc [23,24], Cr [25–27], Mn [24]), $AgFeO_2$ [28,29], $CuCrO_2$ [30], $FeVO_4$ [31,32], $Ba_3SbFe_3Si_2O_{14}$ [33], Fe_3PO_7 [34], and FeP [35] compounds with the spin-modulated structure. It has been shown that the proposed fitting model allows one to not only fairly well describe the experimental spectra but also to extract important information about the spin structure in this ferrite.

II. EXPERIMENTS

The powder Co-substituted samples $BiFe_{1-x}Co_xO_3$ (x = 0.05, 0.1, 0.15) were prepared from a stoichiometric mixture of Bi_2O_3, Co_3O_4, and Fe_2O_3, where approximately 5% of Fe_2O_3, enriched by ^{57}Fe (95.5%), and $KClO_3$ (as the inner source of oxygen) were used. The mixture was placed in a gold capsule and treated at 6 GPa and 1573 K for 2 h in a belt-type high-pressure apparatus. After the heat treatments, the sample was quenched to room temperature, and the pressure was slowly released.

Powder x-ray diffraction measurements were performed on a MiniFlex600 diffractometer using Cu $K\alpha$ radiation (2θ range of 10°−100°, a step width of 0.02°, and a scan speed of 1°/min).

Magnetic measurements were performed on a SQUID magnetometer (Quantum Design, MPMS-XL-7T) from 400 to 2 K and from 2 to 400 K at applied magnetic fields of 100 and 10 kOe.

The ^{57}Fe Mössbauer spectra were performed at 4.7–680 K using a conventional constant-acceleration spectrometer equipped with a helium cryostat (Janis Research SHI-850-5) for low-temperature measurements and a furnace for high-temperature measurements. The ^{57}Co(Rh) radiation source was kept at room temperature (RT). The isomer shifts refer to the α-Fe (at RT). The experimental spectra were analyzed using the SPECTRRELAX software package [36].

III. RESULTS AND DISCUSSION

A. X-ray and magnetic data

X-ray diffraction analysis of the prepared polycrystalline $BiFe_{1-x}Co_xO_3$ (x = 0.05, 0.1, 0.15) samples (see Supplemental Material for XRD patterns, Fig. S1 [37]) evidences the formation of the rhombohedral structure (space group $R3c$), which is usually described in a hexagonal lattice setting [Fig. 1(a)]. The samples contained small amounts of $Bi_2O_2CO_3$ impurity (see Supplemental Material for XRD patterns, Fig. S1 [37]). For further discussion, we note that this structure may be derived from the ideal cubic perovskite lattice by an antiferrodistortive (AFD) out-of-phase tilting of the (FeO_6) octahedron along the $[001]_h$ direction, and shifting of Bi^{3+}/Fe^{3+} along the same direction called an ferroelectric distortion (FE) [2,38] [Fig. 1(b)]. The effect of Co substitution on the $BiFeO_3$ structure can be examined using the refined structural parameters shown in Fig. S2 (see Supplemental Material for parameter dependence [37]). One

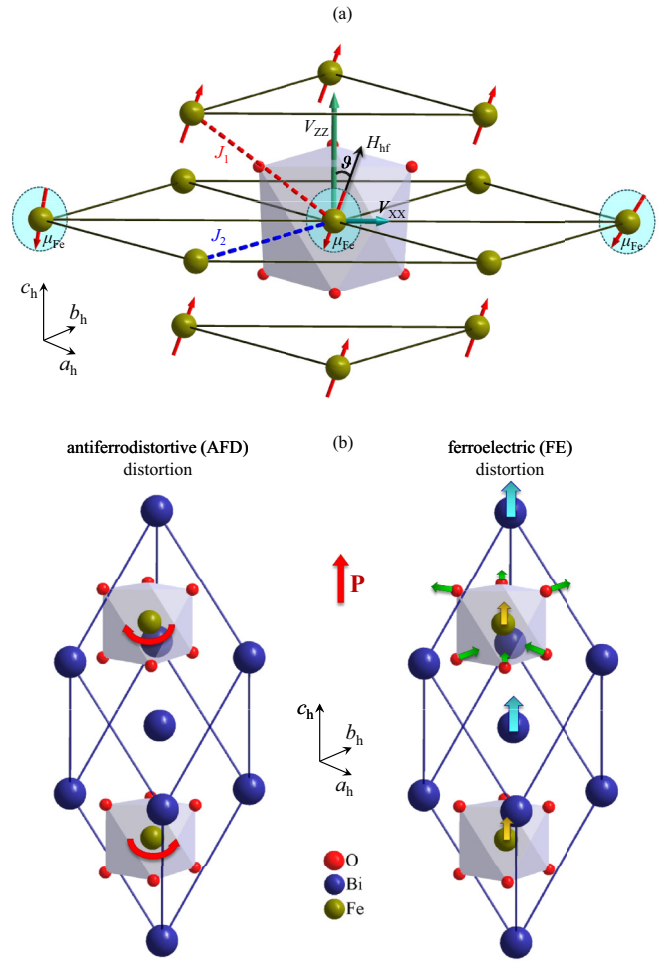

FIG. 1. (a) Schematic view of the local crystal (in hexagonal base) and magnetic structures of the ferrites $BiFe_{1-x}Co_xO_3$. The directions of the principal V_{ZZ} and V_{XX} axes of the EFG tensor (V_{YY} is not shown), magnetic moments of iron ions (μ_{Fe}), and hyperfine field (H_{hf}) at ^{57}Fe nuclei (ϑ is the polar angle of the hyperfine field H_{hf} in the principle axes of the EFG tensor). Shaded ovals indicate the planes of the μ_{Fe} rotation in the cycloidal magnetic structure. The nearest-neighbor (J_1) and next-nearest-neighbor (J_2) interactions are shown. (b) Schematic representation of the antiferrodistortive (AFD) and ferroelectric (FE) distortions. Red and yellow/blue arrows represent the octahedral rotation and shifts (s_{Bi} and t_{Fe}) of ions, respectively. P is electric polarization vector.

can see that hexagonal parameters decrease with an increase in Co concentration (x). This behavior is well consistent with the previous magnetic studies of Co-doped ferrites (x = 0.01, 0.02) interpreted as an effect of replacement of high-spin Fe^{3+} ions (with the ionic radius of 0.64 Å) with smaller LS (0.545 Å) Co^{3+} ions below ∼150 K, and IS (0.56 Å) Co^{3+} above this point [9,10].

The magnetic measurements disambiguate and clearly show the existence of low-temperature magnetic transitions in $BiFe_{1-x}Co_xO_3$ with x = 0.1 and 0.15, with hysteresis on cooling and heating suggesting a phase transition of the first order [Figs. 2(a) and 3(a)]. The transition temperatures were determined from peak positions on the fcc $d\chi T/dT$ versus T curves to be 274 K for x = 0.1 and 190 K for x = 0.15 at

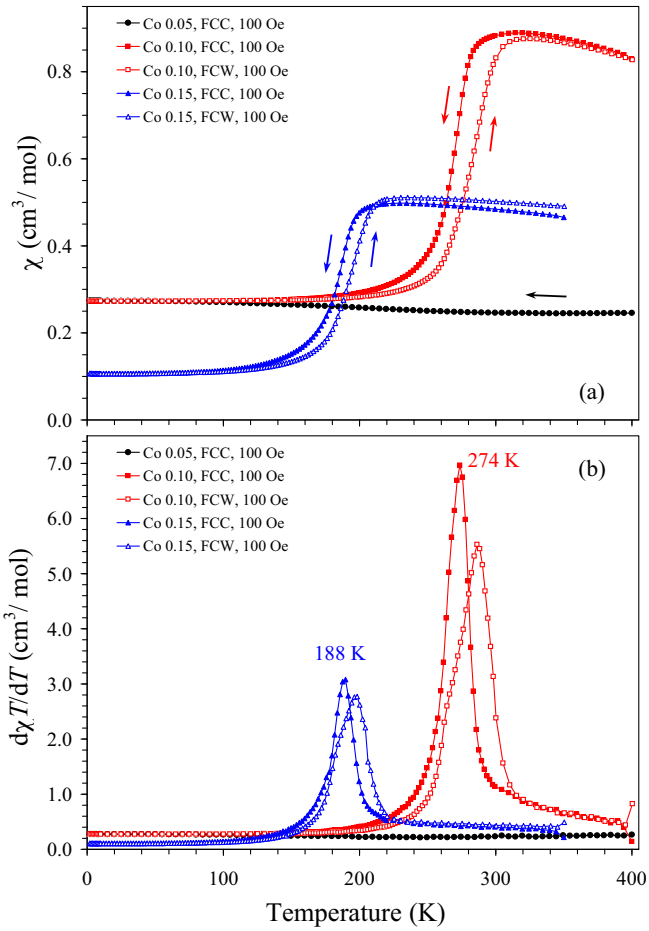

FIG. 2. Dc magnetic susceptibility ($\chi = M/H$) curves of $BiFe_{1-x}Co_xO_3$ with $x = 0.05$ (black), 0.1 (red), and 0.15 (blue) measured at $H = 100$ Oe from 400 K (350 K) to 2 K [field cooled on cooling (FCC): filled symbols] and from 2 to 400 K (350 K) [field cooled on warming (FCW): empty symbols]. (a) χ versus T curves, (b) the same $d\chi T/dT$ versus T curves; peak positions on the FCC curves are marked.

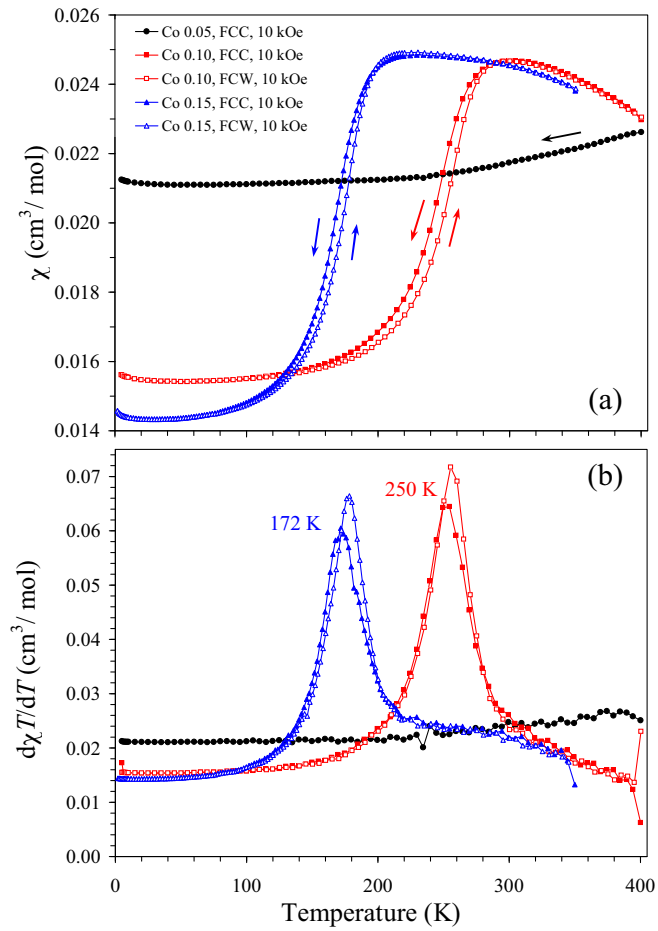

FIG. 3. Dc magnetic susceptibility ($\chi = M/H$) curves of $BiFe_{1-x}Co_xO_3$ with $x = 0.05$ (black), 0.1 (red), and 0.15 (blue) measured at $H = 10$ kOe from 400 K (350 K) to 2 K [field cooled on cooling (FCC): filled symbols] and from 2 to 400 K (350 K) [field cooled on warming (FCW): empty symbols]. (a) χ versus T curves, (b) the same $d\chi T/dT$ versus T curves; peak positions on the FCC curves are marked.

$H = 100$ Oe [Fig. 2(b)], and 255 K for $x = 0.1$ and 172 K for $x = 0.15$ at $H = 10$ kOe [Fig. 3(b)]. The magnetization drops significantly on cooling; this drop approximately corresponds to $1.2\mu_B$/f.u. [calculated as $(8\chi T)^{1/2}$] for both compounds. Therefore, the magnetization change is too large to be explained solely by a spin-state transition of Co^{3+} cations. The drop can probably be related to different spin canting values, which are realized in different magnetic structures below and above the phase transition temperatures. Also the absence of phase transition for the $BiFe_{0.95}Co_{0.05}O_3$ sample can clearly be seen.

B. Mössbauer data

The ^{57}Fe Mössbauer spectra of $BiFe_{1-x}Co_xO_3$ recorded in the paramagnetic temperature range $T \gg T_N$ (see Supplemental Material for additional spectra, Fig. S3 [37]) consist of a single quadrupole doublet with narrow and symmetrical components indicating that iron ions occupy equivalent, or very similar in symmetry, crystal sites. The observed isomer shifts $\delta_{650\,K} \approx 0.14$ mm/s and quadrupole splitting $\Delta \approx 0.44$ mm/s (see Supplemental Material for parameters, Table S1 [37]) correspond to the HS Fe^{3+}($S_{Fe} = 5/2$) ions in an octahedral oxygen environment with a strong electric field gradient (EFG) at ^{57}Fe nuclei. In our previous studies, the principal components of the EFG tensor, $|V_{ZZ}| \geqslant |V_{YY}| \geqslant |V_{XX}|$ at ^{57}Fe nuclei in nonsubstituted ferrite [17], were calculated in order to relate the observed hyperfine parameters with the structure of $BiFeO_3$. It was shown that the large dipole contribution arising from the induced electric dipole moments of Bi^{3+} and O^{2-} ions, in addition to the monopole contribution to the EFG tensor, needs to be taken into account (see Supplemental Material for more details on the model employed [37]). The best agreement between the theoretical and experimental values of quadrupole splittings was found for the polarizability $\alpha_{Bi} \approx 4.0$ Å^3 and $\alpha_O \approx 0.1$ Å^3. The resulting EFG tensor has axial symmetry: $|V_{ZZ}| > |V_{YY}| = |V_{XX}|$. While the $\alpha_O \approx 0.1$ Å^3 is lower than the expected value [17], this results from the strong correlation between α_{Bi} and α_O taken into account and does not affect the directions of the main EFG components and its signs. The positive principal component V_{ZZ} is oriented along

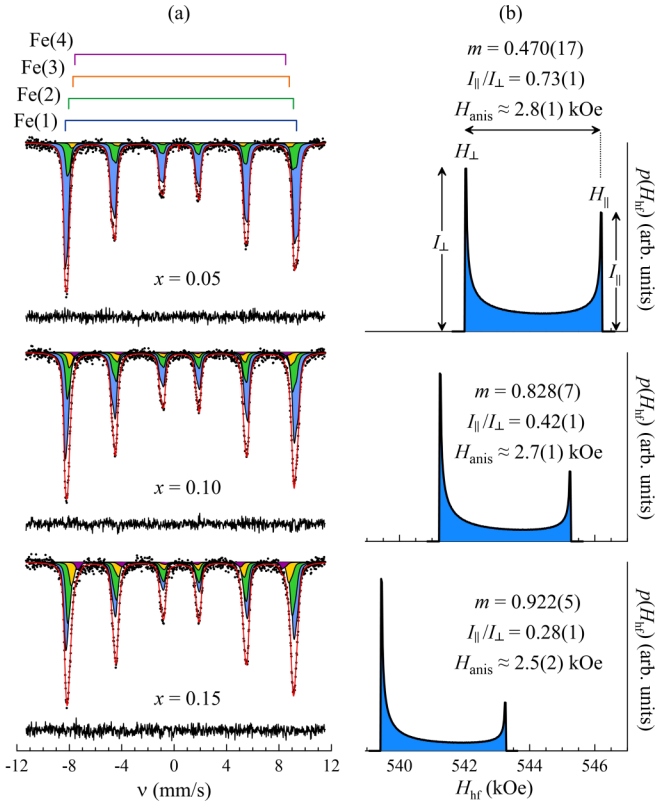

FIG. 4. (a) ^{57}Fe Mössbauer spectra of $BiFe_{1-x}Co_xO_3$ ($x = 0.05$, 0.1, 0.15) recorded at 4.7 K ($T \ll T_N$), and fitted within cycloidal spin model (the red solid line) as described in the text. The Fe(n) subspectra corresponding to the most probable local configurations $\{(6-n)Fe^{3+}; nCo^{3+}\}$ in the nearest coordination sphere of iron are shown by different colors. (b) Resulting shapes of the hyperfine field distribution $p(H_{hf})$ [the asymmetry of the peaks $I_{||}$ and $I_\perp$ caused by anharmonicity (m) of the cycloidal wave].

the c_h axis, and the $V_{XX}(<0)$ component can be directed along the cycloid propagation vector $k = \delta[110]$ ($\delta \approx 0.0045$ at 300 K [2]) [Fig. 1(a)]. It is reasonable to assume that a small substitution degree (x) does not have a significant effect on the EFG parameters (the sign and direction) at ^{57}Fe nuclei in $BiFe_{1-x}Co_xO_3$. This is in accordance with the experimental values (see Table S1 in the Supplemental Material [37]) of the quadrupole splittings for Co-doped ferrites, which do not differ from those for the parent $BiFeO_3$ [17].

The representative ^{57}Fe Mössbauer spectra collected well below T_N are shown in Fig. 4(a). The spectra are very similar to those for nonsubstituted $BiFeO_3$ [17,19–22]. They consist of a six-line hyperfine pattern with inhomogeneous broadened and asymmetric lines. It was shown earlier [19–22] that the observed line broadening is related to the cycloidal magnetic structure due to the small modulation of the excited state hyperfine energies arising when the hyperfine field $H_{hf}(\vartheta)$ at the ^{57}Fe nuclei is rotating with respect to the principal axis V_{ZZ} of the EFG tensor. For a given orientation of $H_{hf}(\vartheta)$ (or iron magnetic moments $\mu_{Fe} \parallel H_{hf}$) with respect to V_{ZZ} [Fig. 1(a)], one can calculate the hyperfine energies up to the first (δE_i) and second ($\delta^2 E_i$) perturbations for the ith of each of the six Zeeman lines (see Supplemental Material [37] for a detailed description). According to our calculations, the V_{ZZ} axis lies in the $(\bar{1}10)_h$ plane of the μ_{Fe} rotation. A continuous variation in the angle ϑ between 0 and 2π results in homogeneous line broadening. Thus, the observed spectral asymmetry in $BiFe_{1-x}Co_xO_3$ cannot be explained by the cycloidal magnetic structure alone. The experimental spectra should be analyzed assuming the anisotropy of the magnetic hyperfine field H_{hf} at the ^{57}Fe nuclei.

Following the ^{57}Fe nuclear magnetic resonance (NMR) in $BiFeO_3$ [39] and Mössbauer measurements in $BiFeO_3$ [17–22] and $BiFe_{1-x}M_xO_3$ (M = Sc, Cr, Mn) [23–27], the peculiar asymmetric shape of the six-line Zeeman pattern below T_N may be assigned to the anisotropy of the $H_{hf}(\vartheta)$ field rotating in the $(\bar{1}10)_h$ plane [Fig. 1(a)]. The anisotropy of H_{hf} is related to the magnetic hyperfine interaction and does not have to be associated with anisotropy of the μ_{Fe} magnitude along the cycloid propagation. Assuming axial symmetry of the hyperfine coupling tensor the angle dependence of H_{hf} can be written as [21,39,40]

$$H_{hf}(\vartheta) \approx H_{||}\cos^2\vartheta + H_\perp \sin^2\vartheta = H_{is} + H_{anis}\frac{3\cos^2\vartheta - 1}{2}, \quad (1)$$

where $H_{||}$ and $H_\perp$ are the magnitudes of H_{hf} when the magnetic moment of Fe^{3+} is oriented along and perpendicular to the $V_{ZZ} \parallel c_h$ direction, respectively. $H_{is} = \frac{1}{3}(H_{||} + 2H_\perp)$ is the isotropic part of H_{hf}, which is primarily determined by the Fermi contact interaction with s electrons polarized by S_{Fe} spins, $H_{anis} = \frac{2}{3}(H_{||} - H_\perp)$ is the anisotropic contribution, which will be discussed later. In order to describe the anharmonicity (i.e., bunching) of spatial distribution of μ_{Fe} moments, one can use the *Jacobi* elliptic functions [2,41,42]:

$$\cos\vartheta(x) = \mathrm{sn}(\pm[4K(m)/\lambda]x, m), \quad \text{for easy-axis anisotropy } (K_u > 0), \quad (2a)$$

$$\sin\vartheta(x) = \mathrm{sn}(\pm[4K(m)/\lambda]x, m), \quad \text{for easy-plane anisotropy } (K_u < 0), \quad (2b)$$

where x is a coordinate along the direction of the spin wave propagation; $K(m)$ is the complete elliptic integral of the first kind; $0 \leqslant m \leqslant 1$ is the anharmonicity parameter related to the effective anisotropy constant $|K_{eff}| \propto mAK^2(m)/\lambda^2$, where A is the exchange stiffness constant; and λ is the period of cycloidal structure. Depending on the parameter m, the spin modulation changes from a purely circular cycloid ($m = 0$ for $K_{eff} \to 0$) to a square wave ($m \to 1$ for $|K_{eff}| \gg A$), in which spins bunch along one direction. The two possible signs in Eq. (2) correspond to the solutions, differing from each other in terms of direction of reference of the $\vartheta(x)$ value. The sign "+" ($K_{eff} > 0$) corresponds to the anisotropy, which tends to align spins along the V_{ZZ} direction, while sign "−" ($K_{eff} < 0$) corresponds to the anisotropy, which tends to $(\bar{1}10)_h$ perpendicular to the V_{ZZ} direction (assuming the axial symmetry of the EFG tensor, i.e., $V_{XX} \approx V_{YY}$). According to our calculations in $BiFeO_3$, $V_{ZZ} \parallel c_h$; therefore, we will refer to $K_{eff} > 0$ as "easy-axis" and to $K_{eff} < 0$ as "easy-plane" anisotropy.

The experimental spectra of $BiFe_{1-x}Co_xO_3$ were fitted by a superposition of four Fe(n) subspectra

corresponding to the most probable local configurations $\{(6-n)\mathrm{Fe}^{3+}; n\mathrm{Co}^{3+}\}_{(n=0-4)}$ in the nearest coordination sphere of iron. To reduce the number of variables in fitting the linewidths (Γ), isomer (δ), and quadrupole [$\varepsilon(\vartheta)$] shifts (see Supplemental Material [37] for details) shifts and anisotropic fields (H_{anis}) were restricted to be the same for all four Fe(n) subspectra. In addition to this, the anharmonicity parameter m was kept the same for all the subspectra. The last assumption suggests that the observed Fe(n) subspectra correspond to Fe^{3+} with different ionic environments but belonging to the same anharmonic spin-modulated magnetic structure. This model satisfactorily describes the entire series of experimental spectra [see Fig. 4(a) and Supplemental Material [37] for all spectra, Figs. S4(a) and S5(a)]. To visualize the effect of anisotropy ($K_{\mathrm{eff}} \neq 0$) that distorts the circular cycloid, hyperfine field distributions $p(H_{\mathrm{hf}})$ resulting from simulation of the spectra are shown in Figs. 4(b), and S4(b) and S5(b) in the Supplemental Material [37].

Figure 5(a) shows the experimental values of the relative contributions (I_n) for the partial spectra Fe(n), in comparison with binomial distribution $P_6(n) \propto x^n(1-x)^{6-n}$ assuming the random distribution of Co^{3+} over the iron sites. Comparison of the experimental and theoretical values of I_n shows that for $x = 0.05$ the Co^{3+} ions are almost uniformly distributed in the lattice. For $x = 0.1$ and 0.15, the distribution is close to the random one but with some preference for iron to have Fe^{3+} in the closest environment. The slight deviation from the uniform Co distribution is consistent with the cluster glass behavior reported earlier for $\mathrm{BiFe}_{1-x}\mathrm{Co}_x\mathrm{O}_3$ with a small degree of Co doping [13].

We have found that the emergence of Co^{3+} ions in the nearest cationic environment of iron reduces the isotropic contribution H_{is} to hyperfine field H_{hf} [Fig. 5(b)]. In the case of ferric oxides, such as isostructural perovskites $\mathrm{BiFe}_{1-x}M_x\mathrm{O}_3$ (M = Sc, Mn, Cr) [23–27], the largest contribution to H_{is} is produced by the contact Fermi field ($H_{\mathrm{F}} > 0$) due to the $3d$-polarization effects on the s shells (the sign "+" indicates that the direction of H_{F} coincides with Fe^{3+} spin $S_{\mathrm{Fe}} = 5/2$ and is opposite to magnetic moment μ_{Fe}). For the $^6A_1$ configuration of Fe^{3+}, anisotropic orbital (H^{orb}) and dipolar (H^{dip}) fields will be very small in almost undistorted octahedral coordination. The second major contribution came from the supertransferred hyperfine field H_{STHF} produced by spins at the neighboring ion (M) sites by transfer and overlap effects through the intervening oxygen ions [43]. The sign of the H_{STHF} contribution is directly related to the electronic structure of M and the nature (sign) of the exchange interactions Fe-O-M. As one can see from Fig. 6, for a near-neighbor cation with half-filled e_g orbitals [$M = \mathrm{Fe}^{3+}, \mathrm{Co}^{3+}(\mathrm{HS}), \mathrm{Ni}^{2+}$], the H_{STHF} field induced through the ~180° Fe-O-M antiferromagnetic exchange is expected to be positive, and therefore increases the resulting H_{hf}. For the nearest neighbor with empty [$\mathrm{Co}^{3+}(\mathrm{LS})$, Cr^{3+}] or less than half-filled [$\mathrm{Co}^{3+}(\mathrm{IS})$, Mn^{3+}]e_g orbitals the H_{STHF} field will be negative so the observed H_{hf} decreases (Fig. 6). Thus, we conclude that the decrease in the H_{is} value as Co^{3+} appears in the iron environment indicates the LS ($t_{2g}^6 e_g^0$) or IS ($t_{2g}^5 e_g^1$) states with an almost zero momentum μ_{Co}. This conclusion is consistent with the neutron diffraction studies of $\mathrm{BiFe}_{0.8}\mathrm{Co}_{0.2}\mathrm{O}_3$ ($\mu_{\mathrm{Co}} \approx 0.29\,\mu_B$) [7], which suggested the Co^{3+} LS state, and $\mathrm{BiFe}_{0.98}\mathrm{Co}_{0.02}\mathrm{O}_3$,

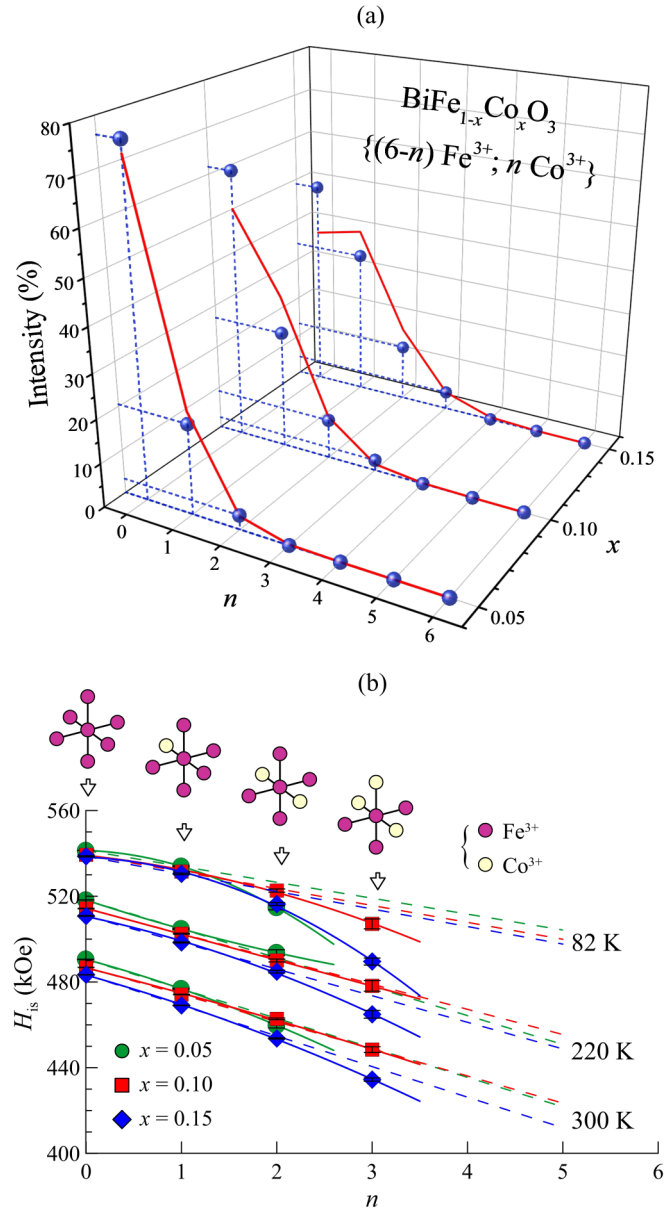

FIG. 5. (a) The experimental values of the relative contributions (I_n) for the partial subspectra Fe(n) (dotted lines are given for better visual perception). Comparison with binomial distribution $P_6(n)$ (red lines). (b) The isotropic part H_{is} ($\equiv 1/3H_{||} + 2/3H_{\perp}$) of the hyperfine magnetic field H_{hf} at ^{57}Fe nuclei as a function of the number of Co^{3+} in the iron surrounding (the upper part of the figure schematically shows some of the possible local iron environments, which correspond to the values of hyperfine fields).

where the LS-IS transition above ~150 K was anticipated [9,10].

The spectra recorded at ~80 K are close to saturation and allow direct determination of the H_{STHF} contribution. To the first approximation, all six exchange Fe-O-Fe interactions can be considered equal, and it is assumed that the change in H_{STHF} when Co^{3+} replaces Fe^{3+} is nearly the same for all six neighboring sites. The observed deviation from the linear dependence $H_{\mathrm{STHF}} = (6-n)h_0$ [Fig. 5(b)] may be associated with the distortion of the nearest oxygen environment in the

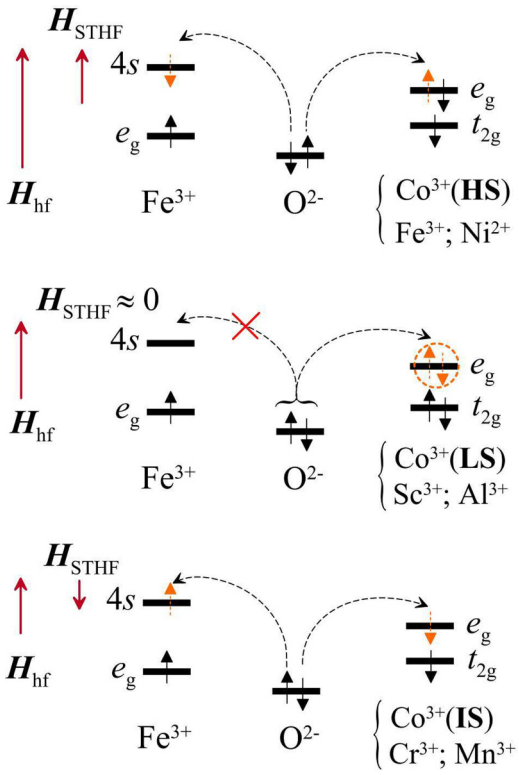

FIG. 6. Schematic diagram for the mechanism of inducing supertransferred hyperfine fields H_{STHF} through electron transfer Fe-O-M (the top panel corresponds to the M^{m+} cations with half-filled e_g orbitals; the middle part of the diagram corresponds to the case of diamagnetic M^{m+}, and the bottom panel corresponds to M^{m+} with the empty e_g orbitals).

(FeO_6) polyhedra as the number of Co^{3+} ions (n) in the iron surrounding increases. The local distortion therefore leads to changes in the angle of exchange bonds Fe-O-Fe(Co), which in turn affect the value of supertransfer contribution (h_0) per Fe^{3+} neighbor. From the Mössbauer data for $BiFe_{1-x}Co_xO_3$ at $T \approx 82$ K [Fig. 5(a)] an average supertransfer contribution $\langle h_0 \rangle = 10(2)$ kOe has been found. This value is consistent with the h_0 value of ~12 kOe deduced for $BiFe_{1-x}Sc_xO_3$ [23] and the theoretical value of about ~15 kOe obtained for perovskitelike orthoferrites [43]. These results confirm our conclusion that Co^{3+} ions in cycloidal arrangement exist in the LS state at low temperatures. Nevertheless, we cannot say anything about the temperature induced spin transition to the IS state of Co^{3+} assumed from magnetic measurements for $BiFe_{1-x}Co_xO_3$ [9,10].

According to our calculations, $V_{ZZ} > 0$, meaning that the maximum value of hyperfine field H_{hf} is attained for the spins of Fe^{3+} ions oriented along the V_{ZZ} axis [Fig. 1(a)]; i.e., $H_{||} > H_{\perp}$. Note that a similar character of hyperfine field anisotropy was observed in the ^{57}Fe NMR spectra for nonsubstituted $BiFeO_3$ ferrite [39]. There are two main anisotropic contributions to the local field H_{hf} of the S-type Fe^{3+} ions with an orbit-nondegenerate state $^6A_{1g}$: the dipole field H^{dip} produced by the neighboring magnetic ions and the anisotropic orbital field H^{orb} generated due to symmetry reduction of the Fe^{3+} wave functions in the low-symmetry crystal fields [28,44].

In the first-order approximation, one may take into account only the projections of anisotropic fields H_{anis} on the direction of the isotropic field H_{is} (taken as the z axis), which exceeds the anisotropic field by several orders of magnitude:

$$\begin{aligned} H^{\mathrm{dip}}(\vartheta) + H^{\mathrm{orb}}(\vartheta) &\approx \frac{3\cos^2\vartheta - 1}{2}\left(H_{\mathrm{an}}^{\mathrm{dip}} + H_{\mathrm{an}}^{\mathrm{orb}}\right) \\ &= \frac{3\cos^2\vartheta - 1}{2}\left\{\mu \sum_k \frac{3\cos^2\alpha_k - 1}{R_k^3} + H_{\mathrm{an}}^{\mathrm{orb}}\right\}, \end{aligned} \quad (3)$$

where ϑ is the angle between the $V_{ZZ} \parallel c_h$ direction and the resultant antiferromagnet vector; k is the summarized index on all positions of neighboring magnetic ions; R_k and μ_k are the module of radius vector $\boldsymbol{R}_k$ and the magnetic moment of the k ion, respectively; and α_k is the angle between R_k and the c_h directions. The substitution of the R_k and α_k values for neighboring iron ions into Eq. (3) made it possible to evaluate dipole fields $\mathrm{H}_{\parallel}^{\mathrm{dip}}(\vartheta = 0)$ and $\mathrm{H}_{\perp}^{\mathrm{dip}}(\vartheta = 90^{\mathrm{o}})$, as well as the anisotropic contributions $\mathrm{H}_{\mathrm{anis}}^{\mathrm{dip}} = \frac{2}{3}(\mathrm{H}_{\parallel}^{\mathrm{dip}} - \mathrm{H}_{\perp}^{\mathrm{dip}})$ (Table I). One can conclude that the anisotropy, $H_{\mathrm{anis}} \approx 2.5 - 2.8$ kOe (at 4.7 K), observed in our experiments cannot be attributed to dipole contribution alone. The most important part of H_{anis} can be related to the anisotropic field $\mathrm{H}_{\mathrm{anis}}^{\mathrm{orb}} = \mathrm{H}_{\mathrm{anis}} - \mathrm{H}_{\mathrm{anis}}^{\mathrm{dip}}$ (Table I) due to "mixing" of the basic state $^6A_{1g}$ and the low-energy excited states ($^4T_{1g}$ or $^6T_{1g}$) resulting from the charge transfer Fe^{3+}–$O^{2-} \rightarrow Fe^{2+}$–$O^{-}(\underline{L})$ ($\underline{L}$ denotes the oxygen hole) [45]. These excited states with a nonzero orbital moment substantially affect the hyperfine field H_{hf} [44]. Perhaps this is the key factor that leads to manifestation of orbital contribution for Fe^{3+} ions in the systems with strong magnetoelectric interactions.

The observed changes in the ^{57}Fe hyperfine structure of $BiFe_{1-x}Co_xO_3$ discussed below can be understood in the framework of the spin Hamiltonian [46]:

$$\left(J_1 \sum_{\langle ij \rangle}^{n.n.} \mathrm{S}_i \cdot \mathrm{S}_j + J_2 \sum_{\langle ij \rangle}^{n.n.n.} \mathrm{S}_i \cdot \mathrm{S}_j\right) + \sum_{\langle ij \rangle} \mathrm{S}_i \cdot \bar{K} \cdot \mathrm{S}_j + \sum_{\langle ij \rangle} \mathrm{d}_{ij} \cdot [\mathrm{S}_i \times \mathrm{S}_j], \quad (4)$$

where the first two terms correspond to the isotropic exchange interaction (E_{ex}); J_1 and J_2 are the isotropic nearest-neighbor (J_1) and next-nearest-neighbor (J_2) interactions [Fig. 1(a)] arising from the large FE distortion of (FeO_6) polyhedra as we discussed before. The second term in Eq. (4) is the magnetocrystal anisotropy (E_{an}), $\bar{K}$ is the anisotropy tensor (in the principal axes system $\{K_{ii}\}_{i=x,y,z}$) and in the case of axial symmetry, $K_u = \frac{1}{3}(K_{xx} + K_{yy} + K_{zz})$ is the constant of the uniaxial anisotropy. The third term is the antisymmetric Dzyaloshinskii-Moriya (DM) interactions; $\boldsymbol{d}_{ij}$ is the antisymmetric DM vector. Usually, one observes the following hierarchy of magnetic interactions $|J_{1,2}| > |K_u| > |d_{ij}|$ [46]. The first two partial contributions tend to establish a collinear magnetic order, while the DM interactions (d_{ij}) deform this order, and make it incommensurate (IC).

TABLE I. Experimental and calculated values of anisotropic hyperfine fields (H_{anis}, H_{anis}^{dip}, H_{anis}^{orb}); anharmonicity parameter (m), and magnetocrystalline anisotropies (K_{eff}, K_{DM}, K_{SI}, K_{dip}).

X	H_{anis} (kOe)	H_{anis}^{dip} (kOe)	H_{anis}^{orb} (kOe)	m	K_{eff} (μeV)	K_{DM} (μeV)	K_{SI} (μeV)	K_{dip} (μeV)
0 [20]	2.91(12)	0.0766	2.83	0.26(6)	0.95(16)	−2.095	1.39(16)	1.663
0.05	2.79(11)	0.0606	2.73	0.47(2)	−1.97(5)	−2.085	−1.20(5)	1.316
0.10	2.67(15)	0.0446	2.63	0.83(1)	−5.49(7)	−2.075	−4.38(7)	0.969
0.15	2.54(21)	0.0286	2.51	0.92(1)	−8.03(9)	−2.065	−6.58(9)	0.622

The important conclusion of this study is that the best fit of the low-temperature spectra can only be obtained by considering bunching of iron spins in the rotation plane $(\bar{1}10)_h$ with the anharmonicity parameter $m \neq 0$ shown in Fig. 7. This observation strongly supports the earlier conclusions from NMR [39] and Mössbauer data for $BiFeO_3$ [17–22] and $BiFe_{1-x}M_xO_3$ (M = Sc, Cr, Mn) [23–27] about the anharmonicity of the spin cycloid, being indicative of the presence of magnetocrystalline anisotropy in the ferrites. The second important piece of information derived from the Mössbauer experiments pertains to the distributions $p(H_{hf})$ at low temperatures, which contain two local maxima of different intensities

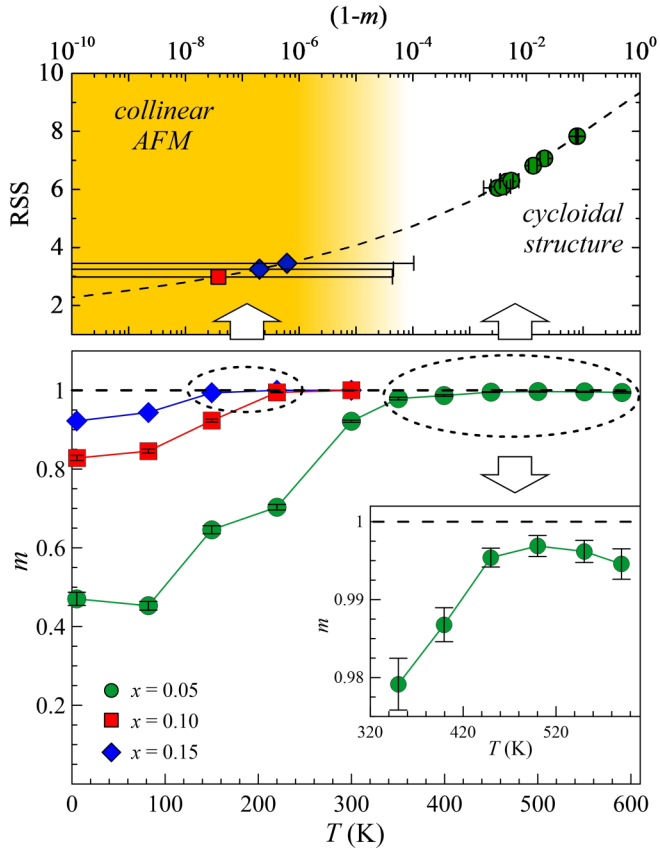

FIG. 7. Temperature dependence of the anharmonicity parameter (m) obtained from the spectra of $BiFe_{1-x}Co_xO_3$. The inset shows some of the points (for the $x = 0.05$ composition) on an enlarged scale of the m axis. The upper panel shows the RSS parameter related to the degree to which the $H_{hf}(\vartheta)$ field projection on the direction of the major axis V_{ZZ} deviates from the square-wave modulation. The RSS parameter is plotted for various values of $(1 - m)$ (see text).

[Fig. 4(b)]. The right one located at $H_{||}$ is characterized by lower intensity ($I_{||}$). This means that the moments $\mu_{Fe} \parallel H_{hf}$ are bunched around the cycloid propagation direction perpendicular to the hexagonal axis c_h (see Supplemental Material for illustration, Fig. S6(a) [37]), which corresponds to the easy-plane magnetic anisotropy, $K_{eff} < 0$, [see Eq. (2)]. It should be noted that nonsubstituted ferrite $BiFeO_3$ (below ~300 K [2,17,19–22]) and substituted ferrites $BiFe_{1-x}M_xO_3$ (M = Sc, Cr, Mn) [23–27] have a cycloidal structure with the easy-axis anisotropy (i.e., $K_{eff} > 0$) (see Fig. S6(b) in the Supplemental Material [37]). In addition, according to the recent neutron diffraction data, $BiFe_{0.98}Co_{0.02}O_3$ nanoparticles with low cobalt content also exhibit an anharmonicity in the commensurate magnetic structure with bunching of magnetic moments along the c_h axis [12]. Hence, the resulting magnetic structure in $BiFe_{1-x}Co_xO_3$ depends on both the size (morphology) of the ferrite particles and content (x) of the cobalt ions.

The substitution of Co for Fe in $BiFe_{1-x}Co_xO_3$ significantly increases the m parameter (Fig. 7), which is associated with a rise of the effective anisotropy constant K_{eff}. The increasing K_{eff} deforms the cycloidal structure forming an inhomogeneous magnetic state, which corresponds to the nearly collinear AFM order in the wide part of the lattice, and the small domain walls where the magnetic moments are reoriented. Our further objective was to use the anharmonicity (m) and magnetic exchange parameters (J_1 and J_2) to directly determine the effective anisotropy constant $|K_{eff}|$, which includes the uniaxial magnetic anisotropy K_u and the anisotropic contribution of the Dzyaloshinskii-Moriya interactions to K_{eff} [22,42,47,48]:

$$K_{eff} = 4m\frac{a_h^2(J_1 - 4J_2)}{\lambda^2}K^2(m) = K_u - \frac{V}{2NS^2}\chi_\perp H_D^2, \quad (5)$$

where a_h is the unit cell parameter in the $(001)_h$ plane; V is the volume of the hexagonal unit cell with six ($N = 6$) high-spin Fe^{3+}($S = 5/2$) ions; $\chi_\perp$ is the magnetic susceptibility in the direction perpendicular to the c_h axis; and H_D is the effective Dzyaloshinskii magnetic field [49]. The effective anisotropy constants $K_{eff}(x)$ were evaluated by substituting the exchange parameters $J_1 = 4.38$ and $J_2 = 0.15$ meV taken for $BiFeO_3$ [46] and the extrapolated cycloid period λ [under the assumption that $\lambda(x)$ linearly changes from 605 Å ($x = 0$) to 630 Å ($x = 0.2$)] [7] into Eq. (5) (Table I). Then, we can use these K_{eff} values to evaluate the uniaxial magnetic anisotropy K_u, by taking typical parameters $H_D \approx 1.2 \times 10^4$ Oe and $\chi_\perp \approx 4.7 \times 10^{-5}$ for $BiFeO_3$ [50] and subtracting their combination from K_{eff}. Assuming that the H_D field and $\chi_\perp$ are practically

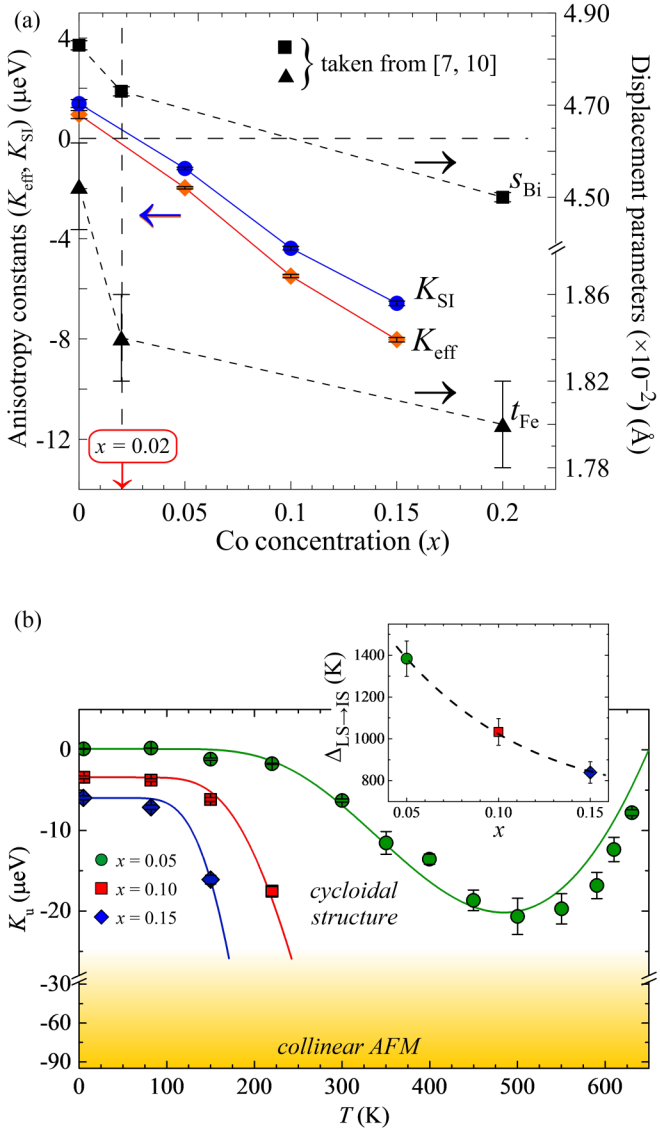

FIG. 8. (a) Dependences of the anisotropy constants ($K_{\rm eff}$ and $K_{\rm SI}$) and shifts of the Bi^{3+}($s_{\rm Bi}$) and Fe^{3+}($t_{\rm Fe}$) ions [7,10] on the Co composition (x) of $BiFe_{1-x}Co_xO_3$. (b) Main panel shows the temperature dependences of the uniaxial anisotropy constants ($K_{\rm SI}$) for the different Co content. Lines indicate the phenomenological fit model as detailed in the text. Inset depicts the energy gap in the LS → IS transition ($\Delta_{\rm LS-IS}$) as a function of the Co content.

independent of Co content, this procedure was carried out for all the samples. The uniaxial anisotropy constants K_u calculated in this way are listed in Table I.

The above calculations illustrated in Fig. 8(b) and Table I have shown that for all the compositions $x > 0.05$ the K_u values are negative and $|K_u|$ increases with Co content in $BiFe_{1-x}Co_xO_3$. According to the theoretical concept [51,52], the magnetocrystalline anisotropy $K_u \approx K_{\rm dip} + K_{\rm SI}$ includes two main components: the magnetic dipole-dipole interaction ($K_{\rm dip}$) and single-ion anisotropy ($K_{\rm SI}$) due to spin-orbit coupling. The $K_{\rm dip}$ contribution is directly related to a very small anisotropic dipole field $H^{\rm dip}$ at ^{57}Fe nuclei: $K_{\rm dip} \approx 15/4\,\mu_B$ $H_{\parallel}^{\rm dip}$ adopted from [53]. Using $H_{\parallel}^{\rm dip}$, one obtains $K_{\rm dip}$, which appears to also be negligible for all compositions (Table I). It means that, in addition to antisymmetric exchange, anisotropy $K_{\rm SI}$ has the strongest effect on the value and sign of magnetocrystalline anisotropy due to the noncubic crystal field and the very small third-order spin-orbit coupling of Fe^{3+} ions. According to the density functional theory (DFT) calculations [54], the competing FE and AFD anisotropic [Fig. 1(b)] deformations in the ferrite $BiFeO_3$ lattice produce easy-axis ($K_{\rm SI} > 0$) and easy-plane ($K_{\rm SI} < 0$) anisotropy, respectively. The resulting sign of $K_{\rm SI}$ is therefore determined by the relative strength of these two distortions. The composition dependence of $K_{\rm SI}$ in $BiFe_{1-x}Co_xO_3$ [Fig. 8(a)] agrees with a decrease in the Bi ($s_{\rm Bi}$) and Fe,Co ($t_{\rm Fe}$) displacements along the c_h axis, as determined by neutron diffraction studies of the compositions with $x = 0-0.2$ compositions [7,10]. The observed lowering of $K_{\rm SI}$ originates from the mutual compensation of opposite-sign anisotropies induced by the FE and AFD distortions. Interestingly, the composition with $x = 0.02$ is close to the transition point where $K_{\rm eff}$ changes its sign and, thus, the total anisotropy energy is strongly reduced [Fig. 8(a)]. This result is the reason for the almost zero anharmonicity parameter $m(\propto K_{\rm eff})$ that was observed in a neutron diffraction study of $BiFe_{0.98}Co_{0.02}O_3$ exhibiting an anharmonic cycloidal structure only at high temperatures $T >$ 50 K (i.e., magnetic anisotropy increases with temperature) [12].

Further insight into the magnetic order in $BiFe_{1-x}Co_xO_3$ was gained from the temperature dependence of the anharmonicity parameter $m(T)$ in the range $4.7 \leqslant T \leqslant T_N$ (Fig. 7). One can see that parameter m increases abruptly with increasing temperature within the range below T^* and tends to the maximal value $m^{\rm max} = 1 (T \rightarrow T^*)$. Visually, this effect manifests itself as a dramatic increase in line asymmetry, $I_\perp > I_{||}$, in the $p(H_{\rm hf})$ distribution [see Fig. 4(b)]. The critical point T^* substantially depends on Co content (x) (Fig. 7). It should be noted that for the composition with $x = 0.05$ in the temperature range $T > T^*$, the anharmonicity parameter $m(T)$ approaches the critical value $m^{\rm max}$ but does not reach it (see the inset in Fig. 5). Furthermore, nonmonotonic changes in the $m(T)$ parameter are observed in this temperature range ($T > T^*$). On the contrary, for the compositions with $x = 0.1$ and 0.15, at $T > T^*$ the $m(T)$ parameter reaches the limiting value $m^{\rm max}$ within the measurement error and then is almost independent of temperature.

The upper panel in Fig. 7 demonstrates two nonoverlapping ranges of the m values for $BiFe_{0.95}Co_{0.05}O_3$ and two ferrites with high cobalt content ($x = 0.1$ and 0.15). The upper panel shows the RSS (residual sum of squares) between the wave function for the particular m value and the rectangle wave (calculated for 200 points) which indicates the parameter related to the degree of deviation of the reduced $H_{\rm hf}(\vartheta)$ field projection on the direction of the major axis V_{ZZ} from the square-wave modulation. It demonstrates that even for high values of $m \sim 0.999$ the modulation remains far above the collinear magnetic structure. One can evaluate the critical anharmonicity parameter and the respective value of the effective anisotropy constant $K_{\rm eff} \sim 0.02-0.03$ meV, above which the magnetic structure of the ferrites becomes collinear leading to the destruction of the cycloid and its transformation into a collinear antiferromagnetic (AFM) G-type structure. It

is important that the magnetic phase transition between the modulated cycloidal structure and collinear G-type ordering was not observed in the parent $BiFeO_3$ and $BiFe_{1-x}M_xO_3$ (M = Sc, Cr) preserving the modulated structure up to the Néel temperature. It is reasonable to suppose that the introduction of Co^{3+} ions into the $BiFeO_3$ lattice produces a more complicated situation than the introduction of either Sc^{3+} or Cr^{3+} ions, since Co^{3+} ions can be stabilized in different spin states and are much more strongly influenced by the crystalline field due to the first-order spin-orbit interaction [55]. Therefore, one can expect that Co doping will have a greater effect on single-ion anisotropy than doping with Sc^{3+} and Cr^{3+} ions.

The rise in $m(T)$ means that the uniaxial magnetic anisotropy constant $|K_u|$ increases [Fig. 8(b)]. The unusual temperature dependence cannot result from competition between the opposite-sign contributions to the effective anisotropy K_{eff} and their different temperature dependences, as has been discussed earlier for the parent $BiFeO_3$ [22,48] and substituted $BiFe_{0.8}Cr_{0.2}O_3$ [25] ferrites. We anticipate that there is another reason why the anisotropy constant K_u increases with temperature: It is associated with the LS-IS transition of Co^{3+} ions [9,10]. Taking into account that the octahedrally coordinated intermediate-spin $Co^{3+}(t_{2g}^5e_g^1)$ ions are characterized by the electronic term $^3T_{1g}$ with nonzero orbital moment, an increase in the temperature population of the excited IS state of the Co^{3+} ions should also lead to anisotropy growth. We can express the temperature dependences of $K_{\text{dip}}(T)$ and $K_{\text{SI}}(T)$ in the molecular field approximation [52]:

$$K_u \propto K_{\text{dip}}(0)B_S^2(y) + [K_{\text{SI}}(0) + x\xi e^{-\Delta_{\text{LS-IS}}/k_BT}]Y(T)$$
$$Y(T) = \frac{1}{2S-1}\left[2(S+1) - 3B_S(y)\frac{1}{2S-1}\coth\left(\frac{y}{2S}\right)\right], \quad (6)$$

where $B_S(y)$ is the Brillouin function for spin quantum number S; $y = [3S/(S+1)](T_N/T)B_S(y)$; $\Delta_{\text{LS-IS}}$ is the energy gap in the LS → IS transition (taken as a fitting parameter). Hence, fitting of the experimental $K_u(T)$ curves for $x = 0.05$, 0.10, 0.15 [Fig. 8(b)] appears to be successful with this interpretation. It is interesting to note that the energy gap values of $\Delta_{\text{LS-IS}}$ decrease with increasing Co content [see the inset in Fig. 8(b)]. From fitting the preexponential factor $\xi \approx (2S+1)K_{\text{Co(IS)}}$, we can evaluate the contribution to the anisotropy from the IS Co^{3+} ions, $K_{\text{Co(IS)}} = -0.33(8)$ meV.

A possible physical reason for the stabilization of the IS state at high temperatures may be understood taking into consideration the strong $3d(\text{Co})-2p(\text{O})$ hybridization [56]. Due to the hybridization, the high-valent cobalt ions have a tendency to have a $3d$-shell occupancy d^7, which corresponds to a formal Co^{2+} valence with the extra hole ($\underline{L}$) located on an oxygen ion. Among the possible charge-transfer configurations, the $t_{2g}^5e_g^2(\underline{L})$ configuration has the lowest energy, thus giving a total IS state. Therefore, the temperature induced nonmagnetic → magnetic transition of Co^{3+} in $BiFe_{1-x}Co_xO_3$ most probably occurs not between LS and HS states, but between LS and IS states. Whether the preferred Co^{3+} spin orientation is parallel to the local Z axis

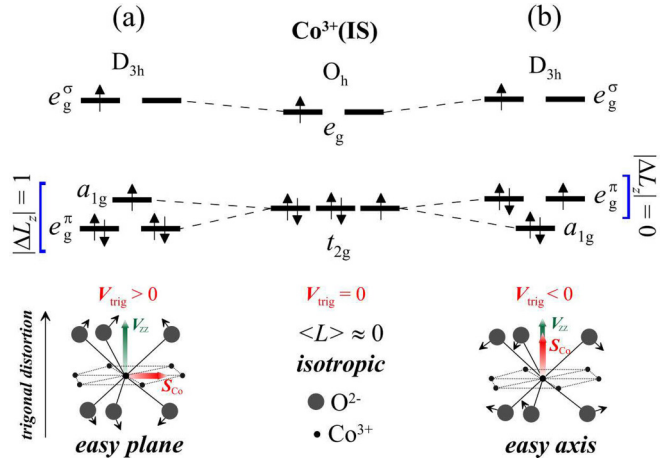

FIG. 9. A schematic view of the intermediate-spin electron configurations of Co^{3+} (d^6, $S_{\text{Co}} = 1$) in the trigonal distorted octahedral surrounding (CoO_6): (a) elongated, $V_{\text{trig}} > 0$, and (b) compressed, $V_{\text{trig}} < 0$, octahedron along the $V_{ZZ} \parallel c_h$ direction (black arrows represent the oxygen shifts). Blue square brackets indicate the $|L, L_z\rangle$ and $|L, L'_z\rangle$ states interacting due to the spin-orbit coupling: $|\Delta L_z| = 1$ (easy-plane anisotropy, $S_{\text{Co}} \perp c_h$) and $|\Delta L_z| = 0$ (easy-axis anisotropy, $S_{\text{Co}} \parallel c_h$).

($\parallel V_{ZZ}$, easy axis) or perpendicular to it ($\perp V_{ZZ}$, easy plane) depends on the value of $|\Delta L_z|$,where $\Delta L_z = L_z - L'_z$ is the difference between magnetic quantum numbers (L_z and L'_z) of two $|L, L_z\rangle$ and $|L, L'_z\rangle$ interacting states due to the spin-orbit (SO) coupling [55]. For the a_{1g} and e_g^π orbitals, $|\Delta L_z| = 1$, the interaction energy $\langle e_g^\pi|\hat{H}_{\text{SO}}|a_{1g}\rangle$ becomes maximum for the $\perp Z$ orientation [Fig. 9(a)]; for the case of two degenerate e_g^π orbitals, $|\Delta L_z| = 0$ [Fig. 7(b)], $\langle e_g^\pi|\hat{H}_{\text{SO}}|e_g^\pi\rangle$ is maximum for the Co^{3+} with $\parallel Z$ orientation. Therefore, the sign of $K_{\text{Co(IS)}}$ in the total anisotropy depends on the sequence of the doublet e_g^π and singlet a_{1g} levels resulting from the trigonal distortion (D_{3h}) of the regular (CoO_6) octahedron along the z direction. The correct sign of the trigonal crystal field (V_{trig}) determining which of the e_g^π and a_{1g} levels has the lowest energy comes from a delicate balance between the nearest O^{2-} and Co^{3+} ions, as well as the electric dipoles of O^{2-} ions [57]. Our further research will address this subject, which requires quantitative calculations.

As mentioned above, the anharmonicity parameter $m(T)$ for $BiFe_{0.95}Co_{0.05}O_3$ in the entire temperature range under study, including $T > T^*$, is not equal to 1. This means that at low cobalt content, the cycloidal structure is retained even at high temperatures but is characterized by a very high degree of anharmonicity $m \to 1$ at $T > T^*$. Figure 10(a) shows the spectra of this ferrite recorded in a broad temperature range. To visualize the effect of the uniaxial anisotropy that distorts the circular cycloid, the projection $H_z \propto H_{\text{hf}}(\vartheta)\text{sn}([4K(m)x/\lambda], m)$ on the $[110]_h$ cycloid propagation is shown in Fig. 8(b). The observed changes in the spectrum profile (e.g., the intensities of external 1,6 lines) with temperature show that the anisotropy field $H_{\text{anis}} \propto (H_{\parallel} - H_{\perp})$ changes its sign at ~400 K. This unusual behavior of $H_{\text{anis}}(T)$ is related to the difference in temperature dependence of fields $H_{\parallel}(T)$ and $H_{\perp}(T)$, but the reason for this difference remains unknown so far. The nonmonotonic changes in the anisotropy

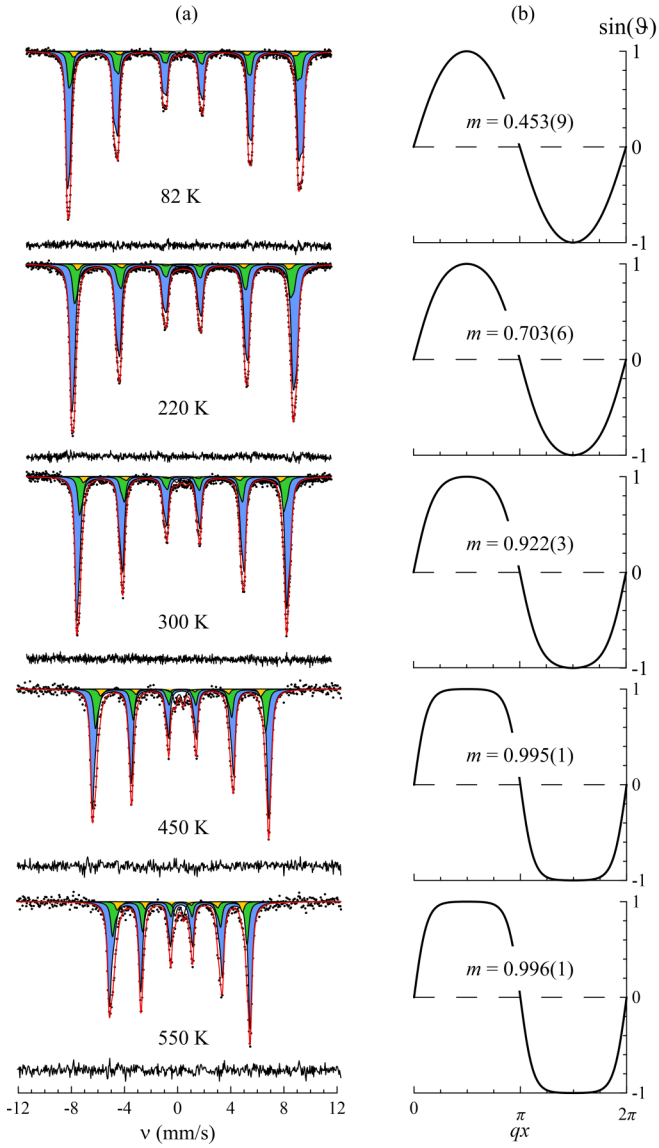

FIG. 10. (a) ^{57}Fe Mössbauer spectra of $BiFe_{0.95}Co_{0.05}O_3$ recorded at the indicated temperatures in the $T < T_N$ interval, and fitted within the cycloidal spin model (the red solid line) as described in the text. (b) Modulation of the projection $H_z \propto H_{\rm hf}(\vartheta)\mathrm{sn}([4K(m)x/\lambda], m)$ on the $[\bar{1}10]_h$ cycloid propagation.

constant $K_u(T)$ [Fig. 8(b)] derived from the experimental dependence $m(T)$ are fitted well by Eq. (6). The emergence of a minimum on the $K_u(T)$ curve is related to the fact that at $T < 500$ K, the population of the IS state increases with temperature and so does $K_{\rm SI}$. Visually, this effect manifests itself as a squared modulation of the projection $H_z(qx)$ [Fig. 10(b)]. The decline in $K_{\rm SI} \propto Y(T)$ with increasing temperature starts to be predominating at higher temperatures (above ~500 K). Since temperature dependences of the anisotropy constant $K_u(T)$ for three different compositions of $BiFe_{1-x}Co_xO_3$ have been qualitatively described using the same approach, the proposed semiquantitative model can be considered self-consistent.

The spectra of $BiFe_{0.9}Co_{0.1}O_3$ and $BiFe_{0.85}Co_{0.15}O_3$ at $T^* < T < T_N$ are shown in Fig. 11. In this temperature

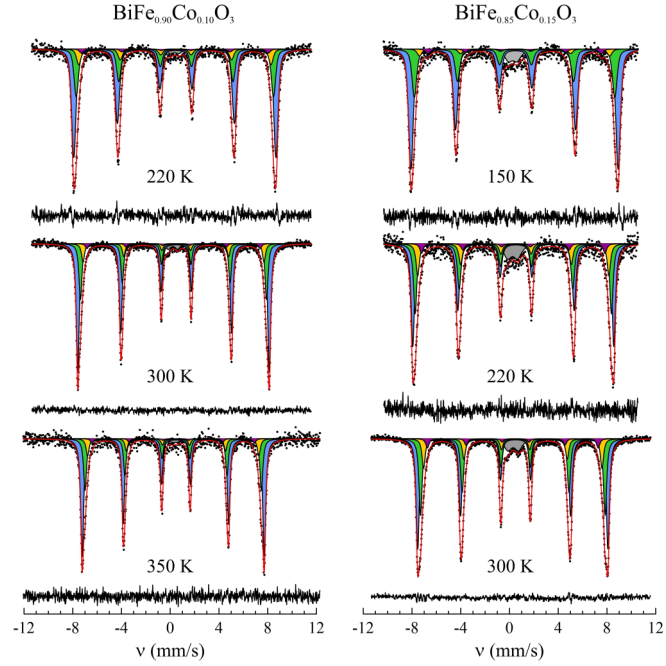

FIG. 11. ^{57}Fe Mössbauer spectra of $BiFe_{0.9}Co_{0.1}O_3$ and $BiFe_{0.85}Co_{0.15}O_3$ recorded at the indicated temperatures in the $T^* < T < T_N$ range, and fitted (the red solid line) within the "discrete" model as a superposition of several Zeeman patterns (as described in the text).

range, all spectra were fitted using a "discrete" model as a superposition of four Zeeman sextets with broadened but symmetrical components, thus attesting to the collinear spin order. One can note the appearance of the small intensity nonmagnetic quadrupole doublet (~3%) in the center of the spectra (Fig. 11), which can be associated with Co-enriched clusters, where iron ions have a nonmagnetic or highly frustrated behavior.

From the observed quadrupole shift of the magnetic component value, one can obtain information about the direction of the $\mu_{\rm Fe}$ moments with respect to the crystal axes. When the ^{57}Fe nuclei experience combined hyperfine interactions, if $H_{\rm hf} \gg eQV_{ZZ}$, the first-order quadrupole shift of energy level is defined as [58]

$$\varepsilon(\vartheta) = (-1)^{|m_I|+1/2}\left(\tfrac{1}{8}eQV_{ZZ}^{\rm par}\right) \times [3\cos^2\vartheta - 1 + \eta\sin^2\vartheta\cos 2\varphi], \quad (7)$$

where $m_I = \pm 3/2; \pm 1/2$ are the nuclear magnetic quantum numbers; $eQV_{ZZ}^{\rm par}$ is the quadrupole splitting constant, which equals that in the paramagnetic range ($T > T_N$) if there is no distortion of the crystal lattice; and θ, φ are the polar angles of the $H_{\rm hf}$ direction in the (XYZ) frame, which is defined by the main axes of the EFG tensor [Fig. 1(a)]. Since Fe^{3+} ions occupy sites with $V_{XX} \approx V_{YY}$ in $BiFe_{1-x}Co_xO_3$, the asymmetry parameter η was taken to be zero; the spectrum shape does not depend on the azimuthal angle φ. By substituting the experimental positive quadrupole shifts $\varepsilon(\vartheta)$ ($T^* < T < T_N$) and quadrupole splittings $\Delta = \frac{1}{2}eQV_{ZZ}^{\rm par}$ ($T > T_N$) into Eq. (7), the angle (ϑ) between the hyperfine field $H_{\rm hf}$ direction and the c_h axis is determined to be ~90°. Therefore,

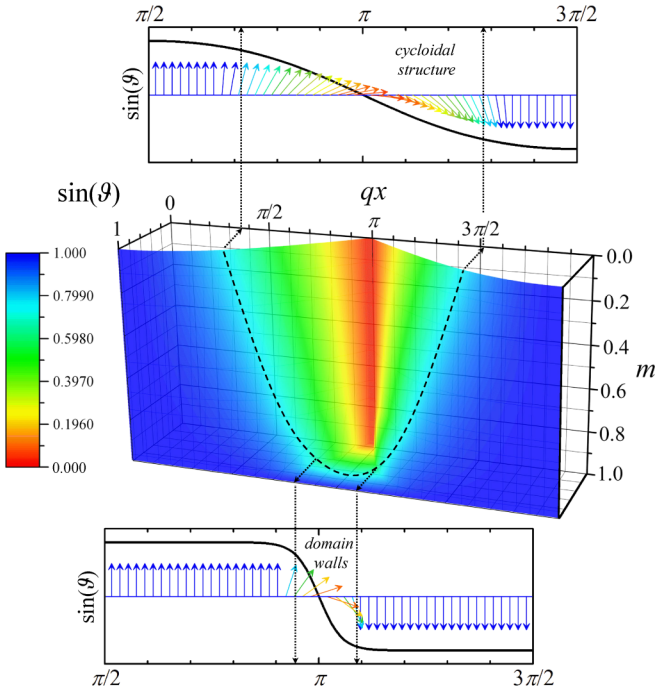

FIG. 12. The angular distribution of magnetic moments of ferric ions through the cycloid propagation λ (horizontal axis) and its anharmonicity m (perpendicular axis) represented as a color map. In the upper and lower panel, the modulation of the hyperfine magnetic field corresponding to the projection (H_z) of $H_{\rm hf}$ on the cycloid propagation is shown.

we can definitely conclude that for all the compositions with $x = 0.10$ and 0.15, the Fe magnetic moments in the collinear antiferromagnetic G-type phase of $BiFe_{1-x}Co_xO_3$ ($T > T^*$) are perpendicular to the hexagonal c_h axis. This result agrees with the neutron diffraction data for $BiFe_{0.8}Co_{0.2}O_3$ showing the transition between the cycloidal magnetic phase and collinear G-type antiferromagnetic ordering with the $\mu_{\rm Fe} \perp c_h$ above $T^* = 100-120$ K [7].

Based on the above Mössbauer data, we cannot confirm the earlier hypothesis that the magnetic phase transition is a first-order phase transition [8]. According to our data for $x = 0.10$ and 0.15 (Fig. 7), the value of m smoothly changes with temperature reaching $m^{(\max)} \approx 1$ above T^*. Such a monotonic change in the order parameter (m) is characteristic of phase transition of the second-order [59], rather than the first-order phase transition, where the fraction of the collinear AFM phase increased on heating. The disagreements between our and the previously obtained Mössbauer data for $BiFe_{0.8}Co_{0.2}O_3$ [8] indicate that information extracted from the experimental Mössbauer spectra substantially depends on the model used for their fitting. This statement is illustrated by the diagram in Fig. 12 showing the dependence of the projection $H_z \propto \mathrm{sn}([4K(m)x/\lambda], m)$ on the anharmonicity parameter m. One can see that at $m \approx 1$, it is very difficult to distinguish the inhomogeneous two-phase magnetic state and high anharmonicity in the cycloid, which corresponds to the nearly collinear spin alignment in the wide part of the lattice, except for the small domain wall where the spins are reoriented within the area of about several unit cells (the lower panel in Fig. 12). At $m < 1$, the magnetic moments of ions diverge from each other almost over the entire wave period (see the upper panel in Fig. 12), which corresponds to the spatially modulated magnetic structure.

IV. CONCLUSIONS

In conclusion, we have carried out a detailed ^{57}Fe Mössbauer study of $BiFe_{1-x}Co_xO_3$ ($0 < x \leqslant 0.15$) that allowed us to elucidate different unconventional features of the electronic and magnetic states of Fe^{3+} and Co^{3+} ions. It was shown that at low temperatures ($4.7 \leqslant T \leqslant T^*$), the observed spectrum shapes are consistent with the modulated cycloidal magnetic structure where equivalent iron magnetic moments are rotating within the $(\bar{1}10)_h$ planes with a high anharmonicity value ($m > 0.45$), which tends to align the spins perpendicular to the hexagonal c_h axis (easy-plane type). The analysis of the spectra was carried out assuming the anisotropy of the hyperfine field $H_{\rm hf}$ at ^{57}Fe, which can be associated with the nonzero orbital contribution of Fe^{3+} ions. The decrease in the $H_{\rm hf}$ field as Co^{3+} appears in the iron environment attests to their LS diamagnetic state at low temperatures. The distribution of Co^{3+} is close to random, but there is some preference for iron to have Fe^{3+} ions in its nearest environment. The m parameter increases with temperature to reach its maximum $m \approx 1$ above T^*, which corresponds to a collinear magnetic structure for $BiFe_{1-x}Co_xO_3$ with $x = 0.1$ and 0.15. The magnetic measurements approve the first-order magnetic transition. For the $BiFe_{0.95}Co_{0.05}O_3$ sample, both Mössbauer spectroscopy and the magnetic measurements demonstrate no phase transition above the Néel point. The strong anharmonicity (m) for this sample at high temperatures as associated with the Co^{3+} nature. We believe that although many details are not clear yet, the observed unusual dependence of $m(T) \propto mK^2(m)$ can result from the IS Co^{3+} ($t_{2g}^5 e_g^1$) ions characterized by the electronic term with nonzero orbital moment.

ACKNOWLEDGMENTS

I.S.G. and A.V.S. acknowledge the Russian Science Foundation (Grant No. 19-73-10034) for the financial support. A.A.B. acknowledges JSPS KAKENHI Grant No. JP20H05276; a research grant from Nippon Sheet Glass Foundation for Materials Science and Engineering (40-37); and Innovative Science and Technology Initiative for Security (Grant No. JPJ004596), Acquisition, Technology & Logistics Agency (ATLA), Japan for the partial support.

[1] G. Catalan and J. F. Scott, Adv. Mater. **21**, 2463 (2009).

[2] J.-G. Park, M. D. Le, J. Jeong, and S. Lee, J. Phys.: Condens. Matter **26**, 433202 (2014).

[3] Y. Zhang, Y. Wang, J. Qi, Y. Tian, M. Sun, J. Zhang, T. Hu, M. Wei, Y. Liu, and J. Yang, Nanomaterials **8**, 711 (2018).

[4] C.-H. Yang, D. Kan, I. Takeuchi, V. Nagarajan, and J. Seidel, Phys. Chem. Chem. Phys. **14**, 15953 (2012).

[5] I. Sosnowska, W. Schäfer, W. Kockelmann, K. H. Andersen, and I. O. Troyanchuk, Appl. Phys. A **74**, S1040 (2002).

[6] I. Sosnowska, J. Microsc. **236**, 109 (2009).

[7] I. Sosnowska, M. Azuma, R. Przeniosło, D. Wardecki, W. Chen, K. Oka, and Y. Shimakawa, Inorg. Chem. **52**, 13269 (2013).

[8] H. Yamamoto, T. Kihara, K. Oka, M. Tokunaga, K. Mibu, and M. Azuma, J. Phys. Soc. Jpn. **85**, 064704 (2016).

[9] J. Ray, A. K. Biswal, S. Acharya, V. Ganesan, D. K. Pradhan, and P. N. Vishwakarma, J. Magn. Magn. Mater. **324**, 4084 (2012).

[10] J. Ray, A. K. Biswal, P. D. Babu, V. Siruguri, and P. N. Vishwakarma, Solid State Commun. **220**, 57 (2015).

[11] D. Ricinschi, Jpn. J. Appl. Phys. **52**, 09KB01 (2013).

[12] H. Hojo, R. Kawabe, K. Shimizu, H. Yamamoto, K. Mibu, K. Samanta, T. Saha-Dasgupta, and M. Azuma, Adv. Mater. **29**, 1603131 (2017).

[13] H. Hojo, K. Oka, K. Shimizu, H. Yamamoto, R. Kawabe, and M. Azuma, Adv. Mater. **30**, 1705665 (2018).

[14] J. Ray, A. K. Biswal, and P. N. Vishwakarma, J. Appl. Phys. **117**, 134102 (2015).

[15] S. R. Burns, D. Sando, B. Xu, B. Dupé, L. Russell, G. Deng, R. Clements, O. H. C. Paull, J. Seidel, L. Bellaiche *et al.*, npj Quantum Mater. **4**, 18 (2019).

[16] K. Sen and M. Singh, Int. J. Phys. Appl. **6**, 33 (2014).

[17] A. Sobolev, I. Presniakov, V. Rusakov, A. Belik, M. Matsnev, D. Gorchakov, and I. Glazkova, in *Mössbauer Spectroscopy in Materials Science—2014*, edited by J. Tuček and M. Miglierini, AIP Conf. Proc. No. 1622 (AIP, Melville, NY, 2014), p. 104.

[18] A. Palewicz, T. Szumiata, R. Przeniosło, I. Sosnowska, and I. Margiolaki, Solid State Commun. **140**, 359 (2006).

[19] V. S. Rusakov, V. S. Pokatilov, A. S. Sigov, M. E. Matsnev, and T. V. Gubaidulina, JETP Lett. **100**, 463 (2014).

[20] V. Rusakov, V. Pokatilov, A. Sigov, M. Matsnev, and T. Gubaidulina, JMSE-B **4**, 302 (2014).

[21] V. Rusakov, V. Pokatilov, A. Sigov, M. Matsnev, and T. Gubaidulina, Bull. Russ. Acad. Sci.: Phys. **79**, 708 (2015).

[22] V. S. Rusakov, V. S. Pokatilov, A. S. Sigov, M. E. Matsnev, and A. P. Pyatakov, EPJ Web Conf. **185**, 07010 (2018).

[23] V. S. Rusakov, V. S. Pokatilov, A. S. Sigov, M. E. Matsnev, A. M. Gapochka, T. Yu. Kiseleva, A. E. Komarov, M. S. Shatohin, and A. O. Makarova, Bull. Russ. Acad. Sci.: Phys. **79**, 976 (2015).

[24] V. S. Rusakov, V. S. Pokatilov, A. S. Sigov, M. E. Matsnev, A. M. Gapochka, T. Yu. Kiseleva, A. E. Komarov, M. S. Shatokhin, and A. O. Makarova, Phys. Solid State **58**, 102 (2016).

[25] V. S. Rusakov, V. S. Pokatilov, A. S. Sigov, A. A. Belik, and M. E. Matsnev, Phys. Solid State **61**, 1030 (2019).

[26] V. S. Pokatilov, V. S. Rusakov, A. S. Sigov, A. A. Belik, M. E. Matsnev, and A. E. Komarov, Phys. Solid State **59**, 443 (2017).

[27] V. S. Pokatilov, V. S. Rusakov, A. S. Sigov, and A. A. Belik, Phys. Solid State **59**, 1558 (2017).

[28] A. Sobolev, V. Rusakov, A. Moskvin, A. Gapochka, A. Belik, I. Glazkova, A. Akulenko, G. Demazeau, and I. Presniakov, J. Phys.: Condens. Matter **29**, 275803 (2017).

[29] I. Presniakov, V. Rusakov, A. Sobolev, A. Gapochka, M. Matsnev, and A. A. Belik, Hyperfine Interact. **226**, 41 (2014).

[30] V. S. Rusakov, I. A. Presnyakov, A. M. Gapochka, A. V. Sobolev, M. E. Matsnev, and Yu. O. Lekina, Bull. Russ. Acad. Sci.: Phys. **79**, 971 (2015).

[31] D. Colson, A. Forget, and P. Bonville, J. Magn. Magn. Mater. **378**, 529 (2015).

[32] A. V. Sobolev, I. A. Presnyakov, V. S. Rusakov, A. M. Gapochka, Y. S. Glazkova, M. E. Matsnev, and D. A. Pankratov, J. Exp. Theor. Phys. **124**, 943 (2017).

[33] A. V. Sobolev, A. A. Akulenko, I. S. Glazkova, E. A. Zvereva, N. S. Ovanesyan, M. M. Markina, and I. A. Presniakov, J. Alloys Compd. **797**, 432 (2019).

[34] A. V. Sobolev, A. A. Akulenko, I. S. Glazkova, D. A. Pankratov, and I. A. Presniakov, Phys. Rev. B **97**, 104415 (2018).

[35] A. V. Sobolev, I. A. Presniakov, A. A. Gippius, I. V. Chernyavskii, M. Schaedler, N. Buettgen, S. A. Ibragimov, I. V. Morozov, and A. V. Shevelkov, J. Alloys Compd. **675**, 277 (2016).

[36] M. E. Matsnev and V. S. Rusakov, in *Mössbauer Spectroscopy in Materials Science—2014*, edited by J. Tuček and M. Miglierini, AIP Conf. Proc. No. 1622 (AIP, Melville, NY, 2014), p. 40.

[37] See Supplemental Material at http://link.aps.org/supplemental/10.1103/PhysRevB.101.224409 for detailed methods and additional results.

[38] A. P. Pyatakov and A. K. Zvezdin, Phys.−Usp. **55**, 557 (2012).

[39] A. V. Zalesskii, A. K. Zvezdin, A. A. Frolov, and A. A. Bush, JETP Lett. **71**, 465 (2000).

[40] V. S. Rusakov, V. S. Pokatilov, T. V. Gubaidulina, and M. E. Matsnev, Phys. Met. Metallogr. **120**, 339 (2019).

[41] I. Sosnowska and A. K. Zvezdin, J. Magn. Magn. Mater. **140–144**, 167 (1995).

[42] M.-M. Tehranchi, N. F. Kubrakov, and A. K. Zvezdin, Ferroelectrics **204**, 181 (1997).

[43] C. Boekema, P. C. Jonker, G. Filoti, F. Van Der Woude, and G. A. Sawatzky, Hyperfine Interact. **7**, 45 (1979).

[44] A. S. Karnachev, Yu. I. Klechin, N. M. Kovtun, A. S. Moskvin, and E. E. Solov'ev, J. Exp. Theor. Phys. **51**, 592 (1980).

[45] A. S. Moskvin, I. G. Bostrem, and M. A. Sidorov, J. Exp. Theor. Phys. **77**, 127 (1993).

[46] J. Jeong, E. A. Goremychkin, T. Guidi, K. Nakajima, G. S. Jeon, S.-A. Kim, S. Furukawa, Y. B. Kim, S. Lee, and V. Kiryukhin *et al.*, Phys. Rev. Lett. **108**, 077202 (2012).

[47] A. G. Zhdanov, A. K. Zvezdin, A. P. Pyatakov, T. B. Kosykh, and D. Viehland, Phys. Solid State **48**, 88 (2006).

[48] V. S. Rusakov, V. S. Pokatilov, A. S. Sigov, M. E. Matsnev, and A. P. Pyatakov, Dokl. Phys. **63**, 223 (2018).

[49] A. Moskvin, Condens. Matter **4**, 84 (2019).

[50] Z. V. Gareeva, K. A. Zvezdin, A. P. Pyatakov, and A. K. Zvezdin, J. Magn. Magn. Mater. **469**, 593 (2019).

[51] A. M. Kadomtseva, A. P. Agafonov, M. M. Lukina, V. N. Milov, A. S. Moskvin, V. A. Semenov, and E. V. Sinitsyn, J. Exp. Theor. Phys. **54**, 374 (1981).

[52] C. L. Bruzzone and R. Ingalls, Phys. Rev. B **28**, 2430 (1983).

[53] J. O. Artman, J. C. Murphy, and S. Foner, Phys. Rev. **138**, A912 (1965).

[54] C. Weingart, N. Spaldin, and E. Bousquet, Phys. Rev. B **86**, 094413 (2012).

[55] M.-H. Whangbo, H. Xiang, H.-J. Koo, E. E. Gordon, and J. L. Whitten, Inorg. Chem. **58**, 11854 (2019).

[56] M. A. Korotin, S. Yu. Ezhov, I. V. Solovyev, V. I. Anisimov, D. I. Khomskii, and G. A. Sawatzky, Phys. Rev. B **54**, 5309 (1996).

[57] J. Smit, F. K. Lotgering, and R. P. van Stapele, J. Phys. Soc. Japan **17**, Suppl. B-I, 268 (1962).

[58] H. Onodera, A. Fujita, H. Yamamoto, M. Sagawa, and S. Hirosawa, J. Magn. Magn. Mater. **68**, 6 (1987).

[59] D. Khomskii, *Basic Aspects of the Quantum Theory of Solids: Order and Elementary Excitations* (Cambridge University Press, Cambridge, 2010).